IAEA ATF-TS BENCHMARK FOR SIMULATION OF BUNDLE TESTS

J. STUCKERT[1], Z. HOZER[2], A. KHAPERSKAIA[3], K. SIM[3],

[1]Karlsruhe Institute of Technology, Karlsruhe, Germany
[2]HUN-REN Centre for Energy Research (HUN-REN EK)
[3]Nuclear Energy Department, IAEA, Vienna International Centre, Wagramer Strasse 5, PO Box 100, 1400 Vienna, Austria

**Corresponding author: juri.stuckert@kit.edu*

ABSTRACT

Since 2021, IAEA has been organizing a Coordinated Research Project (CRP) on Testing and Simulations of Accident Tolerant and Advanced Technology Fuels (ATF-TS). A work sub-task WT2.2 is dedicated to benchmark the integral computer codes used for simulation of bundle tests with ATF cladding materials. The following three bundle tests, carried out under severe accident conditions, were selected for the simulation: CODEX-ATF (HUN-REN EK/Hungary) and DEGREE (CRIEPI/Japan) both with chromium coated Zr-alloy cladding tubes, and QUENCH-19 (KIT/Germany) with FeCrAl cladding tubes. Seven organizations using six different codes took part in the post-test simulation of the QUENCH-19 test. The preparation of the CODEX-ATF test was based on calculations carried out with three codes in three organizations; four organizations are participating in the post-test simulation currently underway. Four institutes with four different integral codes were participated in the pre- and post-test modelling of the DEGREE-B3 bundle test.

This paper presents briefly the chosen bundle tests, the participants and codes used, and a comparison of the simulation results.

1. Introduction

As part of the IAEA ATF-TS project, not only numerous single rod tests were carried out with ATF materials, but also two bundle tests with Cr coated claddings made of Zr alloys: the DEGREE-B3 bundle test at CRIEPI [1] and CODEX-ATF test at HUN-REN EK [2]. The advantage of bundle tests lies in the creation of prototypical adiabatic conditions and the possibility of studying the mutual influence of fuel rods. In addition, such integral tests are a good basis for verification and validation of computer codes. Therefore, it was decided to conduct a benchmark within the framework of this IAEA project using experimental data obtained both during tests and in post-test studies. In addition to the two bundle tests using chromium-coated zirconium claddings, it was proposed to also use the results of the QUENCH-19 bundle test with FeCrAl claddings previously conducted at FZK. Conducting benchmark for the QUENCH-19 test was initiated within the framework of the previous IAEA ACTOF project [3], but then only two research organizations managed to take part in this project. Now the range of organizations involved has been significantly expanded.

2. Benchmark on the QUENCH-19 bundle test performed with FeCrAl claddings

The QUENCH-19 bundle experiment with 24 B136Y cladding tubes and 4 Kanthal AF spacer grids as well as 7 KANTHAL APM corner rods and KANTHAL APM shroud was conducted at KIT on 29th August 2018 [4]. This was performed in cooperation with the Oakridge National Laboratory (ORNL). The test objective was the comparison of FeCrAl(Y) and ZIRLO claddings under similar electrical power and gas flow conditions. The experiment was performed in four stages. The electrical power supply was the same as in the reference test QUENCH-15 (ZIRLO) during the first two stages (pre-oxidation and transient). The third stage with constant electrical power was performed to extend the temperature increase period. The test was terminated at peak cladding temperature of about 1460 °C by water flooding similar to QUENCH-15. The total hydrogen production was 9.2 g (47.6 g for QUENCH-15).

Seven organizations provided results for exercises on the modelling of the QUENCH-19 bundle test (Table 1).

Partici-pant	CNEA Argentina	CTU Czech Republic	GRS Germany	IBRAE Russia	KIT/INR Germany	NINE Italy	UPM/NFQ Spain
Code	DIONISIO	MELCOR	ATHLET-CD	SOCRAT	ASTEC	MELCOR	MELCOR

Table 1. Organizations and codes participated in the QUENCH-19 benchmark

For almost all codes, the rod bundle was described by three concentric rings as shown in Fig. 1: an inner ring (ROD1) containing four central rods, a second ring containing eight intermediate rods (ROD2), and a third ring containing twelve peripheral rods (ROD3). When modeling with the MELCOR code, NINE and CTU applied a division into two groups of fuel rods: internal and external rods. Only one central rod was modelled with the DIONISIO code. The corner zirconium rods used for the bundle instrumentation were taken into account by their effect on reducing the flow area of the assembly. In addition, their outer surface area was taken into account when calculating the hydrogen release due to their oxidation. Also, when calculating the hydrogen release, the influence of the inner surface of the shroud was taken into account.

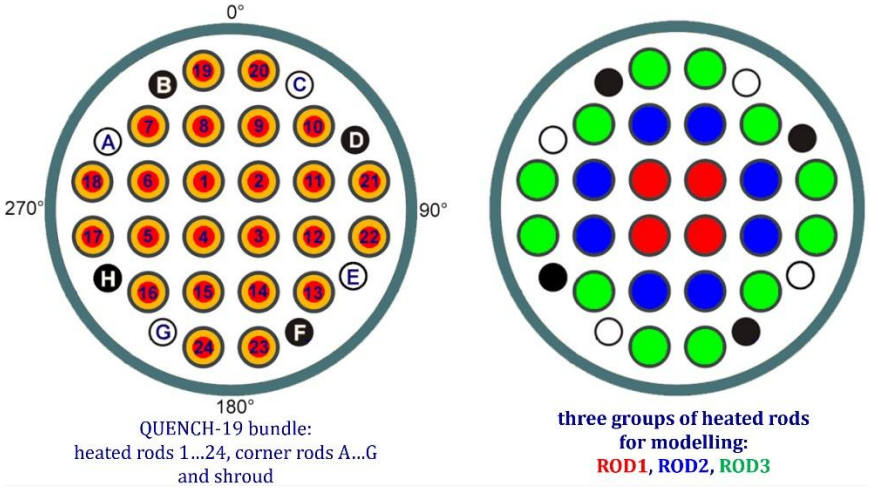

Fig. 1. Composition of the QUENCH-19 bundle

According to the benchmark conditions, each code had to calculate - based on specified boundary conditions and experimental data on the temporary change in electrical power supplied to the bundle - the temperature history at each of the seventeen elevations of the assembly. In addition, the most important parameter for comparing the efficiency of codes should have been the calculated value of hydrogen release.

2.1 Comparison of temperature predictions

Based on the readings of the thermocouples of the central and intermediate rods, an axial distribution of temperatures in the inner bundle part was obtained 300 s before the start of the reflood, namely at the time of 8800 s (in a later period, a number of thermocouples failed). Comparison of these experimental data with the results of calculations shows a good prediction of the position of the maximum temperature at the bundle elevation of 850 mm by most codes (Fig. 2). Below this level, the data from the four codes practically coincide with the experimental data. Above 850 mm, the data of the two codes coincide with the measured values. The other two codes give overpredicted temperature values.

Comparison of calculated temperatures with experimental ones at the bundle elevation of 950 mm throughout the experiment shows overestimated values for all codes - satisfactory for the first (Fig. 3) and second (Fig.4) groups of rods and significantly overestimated for the shroud (Fig. 5). The

latter circumstance may be due to insufficient consideration of the steam-water mixture entering through leaks into the space between the shroud and the cooling jacket surrounding it [4].

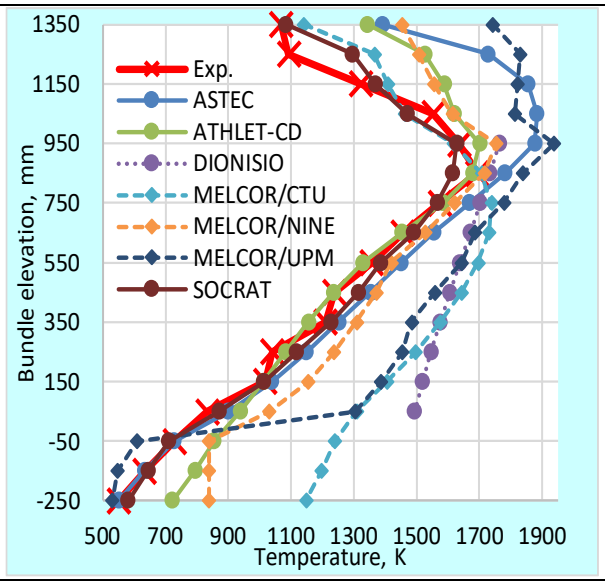

Fig 2. Axial temperature profiles for QUENCH-19

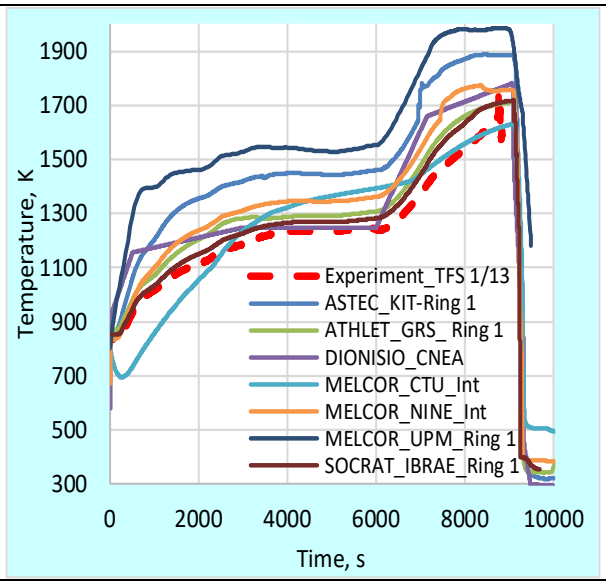

Fig. 3. Temperature progress for internal rods

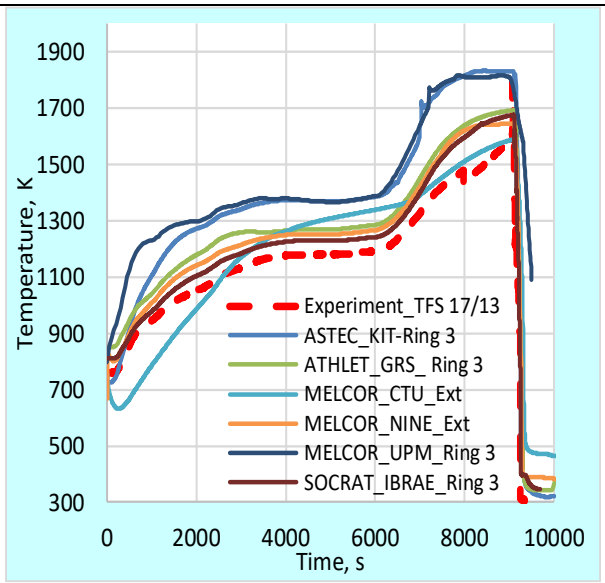

Fig. 4. Temperature progress for external rods

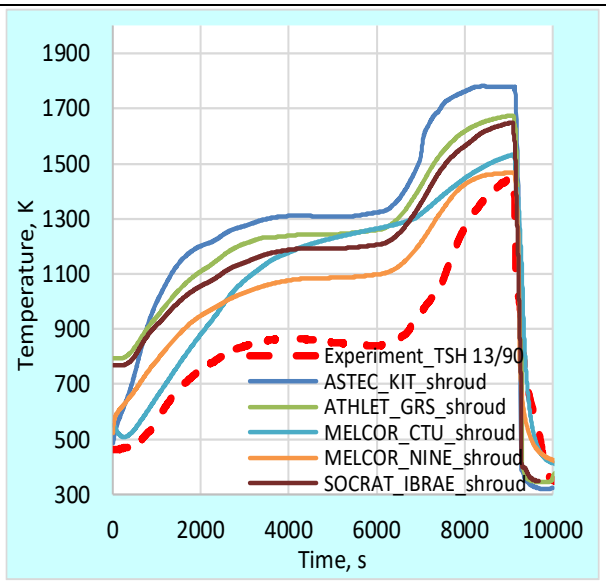

Fig. 5. Temperature progress for shroud

2.2 Comparison of hydrogen predictions

When metal M is oxidized in steam, hydrogen is released, the release rate of which is determined by the degree of oxidation:

$$xM + yH_2O = M_xO_y + yH_2 \quad (1)$$

The enhanced oxidation resistance of FeCrAl alloys at high temperatures relies on the formation of a slowly growing and highly protective Al_2O_3 scale [5]. The formation of a protective alumina scale is determined by the competition between the oxidation rate governed by diffusion of O and Al through the oxide layer and the diffusion of aluminium in the substrate to the interface. Alumina performs its protective role at temperatures below approximately 1650 K. At higher temperatures, accelerated diffusion processes lead to increased Fe oxidation, leading to a catastrophic increase in the oxidation rate. Based on the results of oxidation experiments performed at MIT with the B136Y3 samples (FeCrAl alloy used for the QUENCH-19 claddings) [6], the following correlations for the parabolic rate constant of the sample mass gain have been proposed to use for all codes:

$$K_{MIT}[\frac{g^2}{cm^4 s}] = \begin{cases} 9.62 \times 10^{-12}, & T \leq 1473\ \mathrm{K} \\ A_B \exp\left(\frac{-E_B}{RT}\right), & 1473\ < T < 1648\ \mathrm{K} \\ A_{Fe} \exp\left(\frac{-E_{Fe}}{RT}\right), & T \geq 1648\ \mathrm{K}\ (melting\ point\ of\ FeO) \end{cases} \quad (2)$$

where the activation energies E_B=594354 J/mol and E_{Fe}=352513 J/mol, the pre-exponential constants A_B=3×10^9 g^2/cm^{4}s and A_{Fe}=2.4×10^6 g^2/cm^{4}s.
It should be noted that more detailed experiments carried out later at KIT [7] showed more precise results with the following kinetics for this alloy (derived from data published in [7]):

$$K_{KIT}[\frac{g^2}{cm^4 s}] = \begin{cases} A_L \exp\left(\frac{-E_L}{RT}\right), & 873\ < T < 1173\ \mathrm{K}\ (transient\ alumina) \\ 4.69 \cdot 10^{-14}, & 1173\ \leq T \leq 1273\ \mathrm{K} \\ A_H \exp\left(\frac{-E_H}{RT}\right), & 1273\ < T < 1648\ \mathrm{K}\ (\alpha - alumina) \\ A_{Fe} \exp\left(\frac{-E_{Fe}}{RT}\right), & T \geq 1648\ \mathrm{K}\ (melting\ point\ of\ FeO) \end{cases} \quad (3)$$

where the activation energies E_L=184729 J/mol, E_H=287748 J/mol and E_{Fe}=352513 J/mol, the pre-exponential constants A_L=5375.6*10^{-8}, A_H=6*10^{-2} and A_{Fe}=2.4×10^6 g^2/cm^{4}s.
A comparison of the two oxidation correlations presented in Fig. 6 shows that the correlation obtained from the MIT data is more conservative and thus gives a more conservative estimate for the hydrogen release.

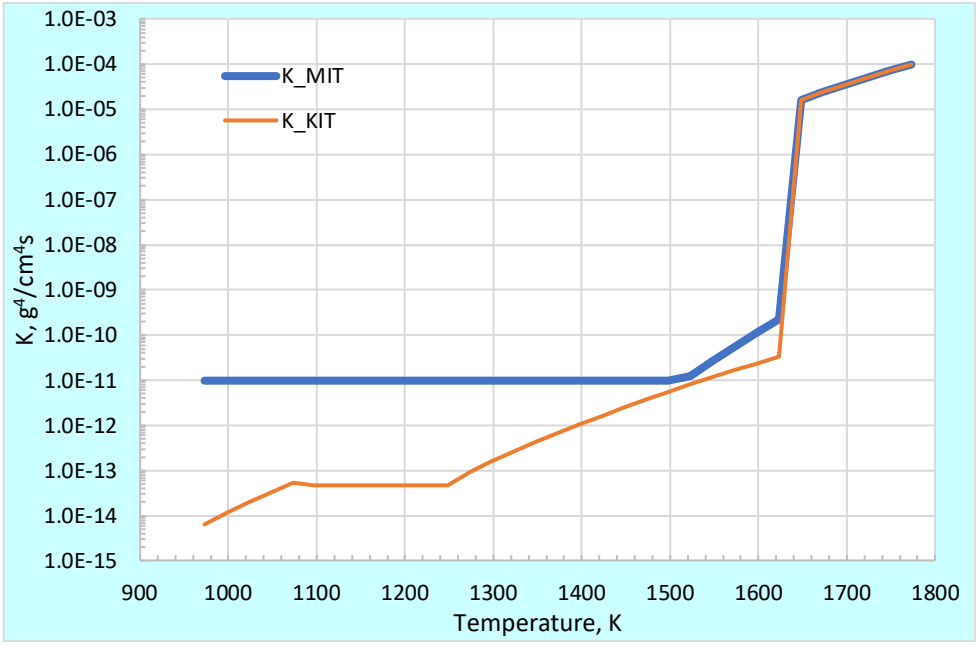

Fig. 6. Comparison of two parabolic rate constants for mass gain during oxidation of the B136Y3 alloy

For the oxidation of KANTHAL alloys (used for shroud and corner rods), it is proposed to use the following correlation established in the temperature range 1323 < T < 1749 K for the KANTHAL APMT alloy [8]:

$$K_A = A_A \exp\left(\frac{-E_A}{RT}\right) \quad (4)$$

where the activation energies E_A=344000 J/mol, the pre-exponential constants A_A=7.84 g^2/cm^{4}s.

All benchmark participants used the proposed oxidation correlations with minor individual adjustments for better matching when transitioning between different temperature intervals. Comparative results for the simulated integral hydrogen release are presented in Fig. 7.

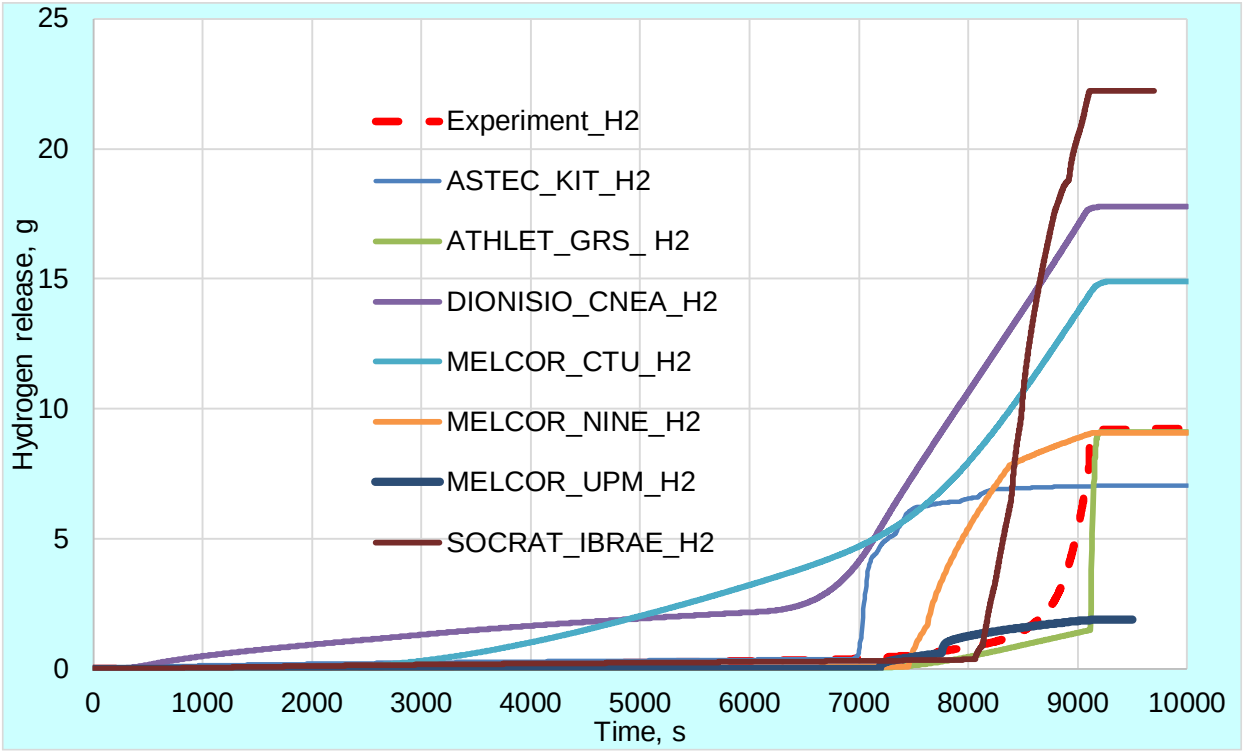

Fig. 7. Simulation results for hydrogen release during the QUENCH-19 bundle test

A very good prediction for the total mass of released hydrogen was given by two codes, which is primarily due to the fairly accurate calculation of bundle temperatures by these codes. The deviation in the prediction of total hydrogen release by other codes is due to either increased calculated temperatures (overprediction of hydrogen) or individual modification of the oxidation correlation for iron (underprediction of hydrogen).

3. Benchmark on the DEGREE-B3 bundle test performed with Cr coated Zry-4 claddings

The DEGREE-B3 bundle experiment with nine Zircaloy-4 cladding tubes with 235 mm length (provided by KIT/Karlsruhe and PVD coated to 20 µm Cr layer by CTU/Prague) was conducted at CRIEPI on 11th April 2023. The inductive heated test bundle was oxidised in a flow of steam/Ar gas mixture under transient conditions up the peak cladding temperature of 1350 °C and then cooled in Ar. Before testing, all nine rods were pressurised with He to 6 MPa and showed symmetrical ballooning and burst during the test, with the middle at the hottest bundle elevation of 135 mm.

Four organizations provided results for exercises on the modelling of the DEGREE-B3 bundle test (Table 2).

Participant	KIT/INR Germany	CRIEPI Japan	IBRAE Russia
Code	ASTEC	FRAPTRAN	SOCRAT

Table 2. Organizations and codes participated in the DEGREE-B3 benchmark

3.1 Comparison of temperature and burst predictions

According to experimental data, the induction heating power during the preparatory stage was 2 kW, then during the bundle heating stage it increased to 23 kW for 430 s, after which the

induction heating was turned off. Tungsten rods installed in the center of each of the nine fuel rod simulators were used as susceptors. However, the alternating magnetic field also excited eddy currents in the cladding tubes, i.e. some of the heat was also generated in the claddings, and not just in the center of the fuel elements. Different considerations of this fact by different codes may cause differences in predictions of thermohydraulic effects.

Since the thermocouples in the bundle were installed at the 125 and 180 mm elevations (below and above the burst positions), temperature simulations were performed for these bundle elevations. The corresponding calculated data are presented in Figs. 8 and 9. The temperature escalation predicted by the SOCRAT code at 125 mm should be associated with the diffusion of chromium into the zirconium matrix, leading to the disappearance of the protective chromium layer and accelerated oxidation of zirconium at this temperature [5, 9].

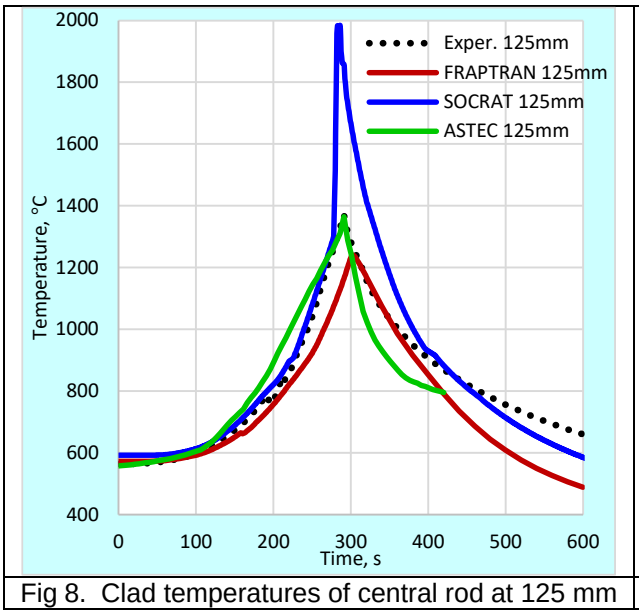

Fig 8. Clad temperatures of central rod at 125 mm

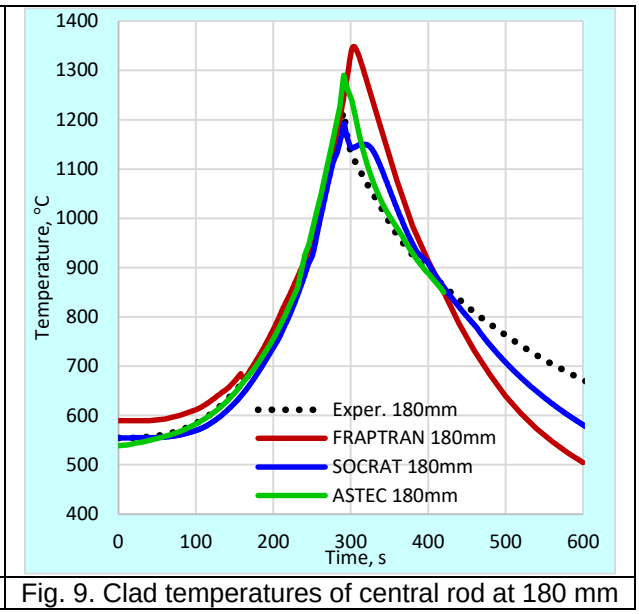

Fig. 9. Clad temperatures of central rod at 180 mm

A detailed account of the dependence of the mechanical properties of the cladding on temperature in the SOCRAT code made it possible to quite accurately predict the burst temperature of the central cladding and the corresponding pressure decrease inside this rod (Fig. 10). The value of this parameter (about 840 K) corresponds to the burst temperatures observed for uncoated Zircaloy-4 claddings [10].

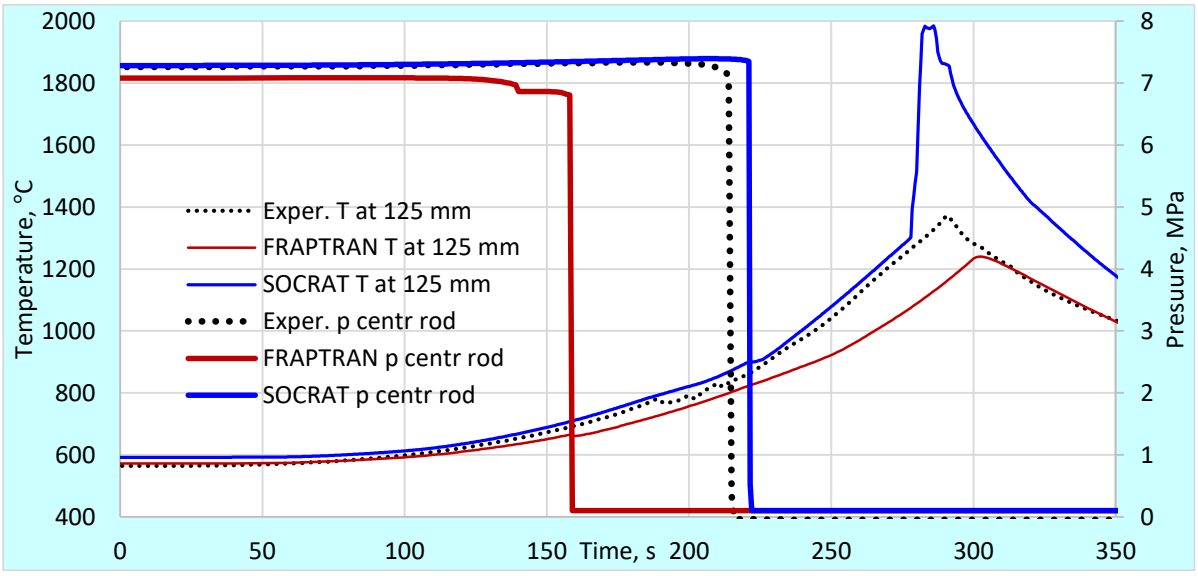

Fig. 10. Pressure progress inside the central rod of the DEGREE-B3 bundle

3.2 Comparison of hydrogen predictions

The oxidation by steam of the chromium results in the formation of a well-adherent and protective Cr_2O_3 layer and a certain amount of hydrogen is released:

$$2Cr+3H_2O=Cr_2O_3+3H_2 \quad (5)$$

The growth kinetics of these oxides can be described by parabolic correlations according to the following correlations:

$$Cr_2O_3 \text{ thickness (derived from the data in [9])} \quad \boldsymbol{\delta}\,[m] = \mathbf{2.63 \cdot 10^{-3} \cdot e^{-\frac{119747}{R \cdot T}} \cdot \sqrt{t}} \quad (6)$$

$$Cr_2O_3 \text{ mass gain } \Delta \boldsymbol{m}\,[\tfrac{kg}{m^2}] = \delta \cdot \rho_{Cr2O3} \cdot \frac{3M_O}{M_{Cr2O3}} = \mathbf{4.327 \cdot e^{-\frac{119747}{R \cdot T}} \cdot \sqrt{t}} \quad (7)$$

where density of chromia ρ_{Cr2O3}=5210 kg/m³, molar mass of oxygen M_O=16, chromia M_{Cr2O3}=152.

These correlations are valid up to a temperature of 1332 °C, after which chromium diffusing into the zirconium matrix forms the Cr/Zr eutectic melt. Taking into account correlation (7), codes FRAPTRAN and ASTEC obtained the hydrogen release shown in Fig. 11. Since FRAPTRAN is a single-rod code, the common hydrogen release from the nine-fuel bundle was calculated by multiplying by 9. Calculations with the SOCRAT code showed an excess of the threshold temperature of 1332 °C, so after reaching this value, the standard Cathcart-Pawel correlation was used for the oxidation of Zircaloy-4 (Fig. 12). From the two presented figures it is clear that taking into account only the oxidation of chromium leads to an underestimation of hydrogen, while inclusion of the kinetics of zirconium oxidation too early gives an overestimated result.

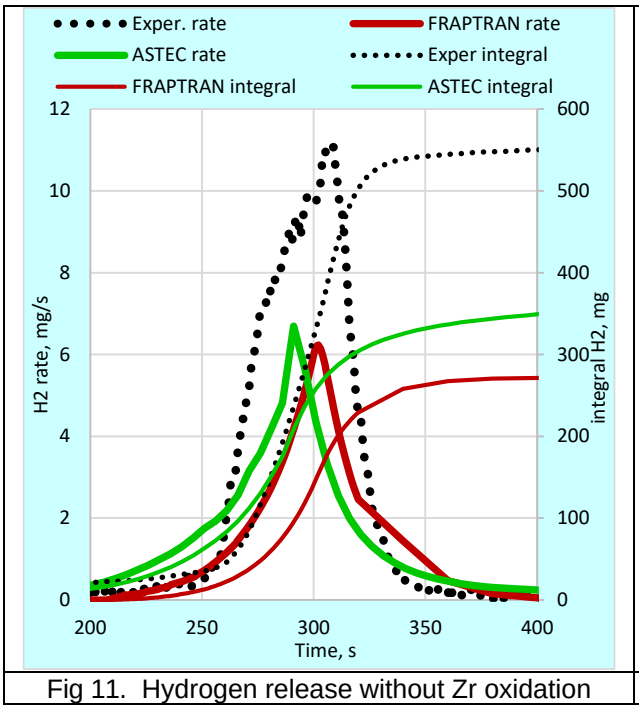

Fig 11. Hydrogen release without Zr oxidation

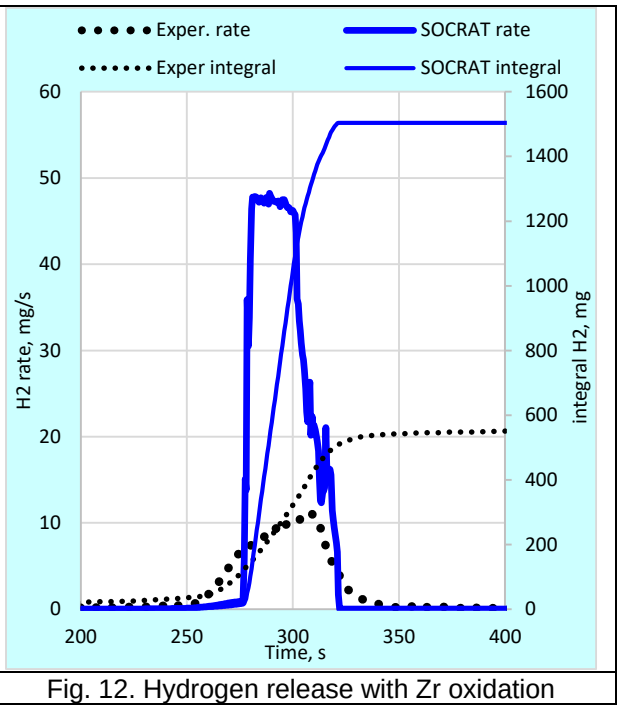

Fig. 12. Hydrogen release with Zr oxidation

4. Benchmark on the CODEX-ATF bundle test performed with Cr coated ZIRLO claddings

The CODEX-ATF bundle experiment with seven electrically heated rods, having opt. ZIRLO cladding tubes with 650 mm length, 9.1 mm outer diameter and 0.58 mm wall thickness, was conducted at HUN-REN EK/Budapest on 11th August 2023. The bundle composition included one centre rod, six peripherical rods, two Zr1%Nb grids with the pitch of 12.75 mm. Four claddings were PVD coated to 20 µm Cr layer by CTU/Prague, three other cladding tubes were not coated. The

bundle was surrounded by Zr2.5%Nb hexagonal shroud. During the test, the bundle was pre-oxidized in Ar/steam atmosphere (each gas 0.2 g/s). The test was terminated by water quench with the water injected from the bundle bottom with the flow rate of 10 g/s.

Four organizations provided results for exercises on the pre- and post-test modelling of the CODEX-ATF bundle test (Table 3).

Participant	CNEA Argentina	GRS Germany	IBRAE Russia	NUBIKI Hungary
Code	DIONISIO	ATHLET-CD	SOCRAT	ASTEC
pre-test		+	+	+
post-test	+	+	+	

Table 3. Organizations and codes participated in the CODEX-ATF pre-test calculations

4.1 Comparison of CODEX-ATF temperature predictions

According to the pre-test specification, the pre-oxidation should be performed at 1000 W bundle power and 800 W power of the shroud heater. The accelerated last transient stage should last 200 s with the bundle power increased to 2000 W. However, commissioning tests carried out after pre-test calculations showed that an increased temperature growth can occur without increasing the bundle power. Therefore, it was decided to carry out the pre-oxidation and accelerated transition stages at a bundle power of 1000 W with an increased duration of the entire experiment. Of course, this led to a deviation of the temperature history from the calculated values. Comparison of calculated temperatures of the central rod with experimental ones at the hottest bundle elevation of 550 mm throughout the experiment shows underestimated values for all codes (Fig. 13).

The post-test calculations showed much more correct results. However, all codes did not reproduce the temperature escalation before quench.

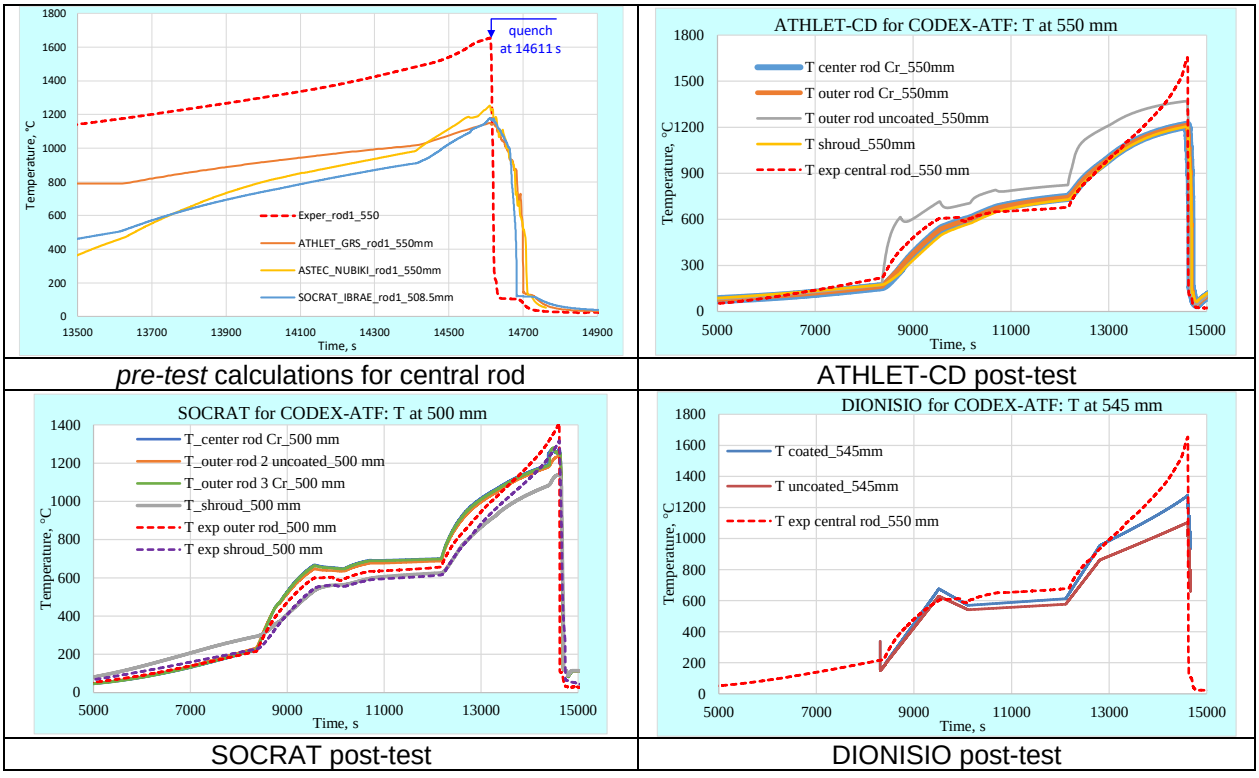

pre-test calculations for central rod | ATHLET-CD post-test

SOCRAT post-test | DIONISIO post-test

Fig. 13. Temperature progress for the central CODEX-ATF rod at the hottest bundle elevation

4.2 Comparison of hydrogen predictions

Because of the seven rods, only four cladding tubes were coated with chromium, the oxidation correlations presented in Chapter 3.2 were applied only to them. In the SOCRAT calculations, the hydrogen produced by the oxidation of coated claddings is due not only to the oxidation of the Cr, but also to the oxidation of the underlying Zr. For the cladding of the three remaining rods and the inner surface of the shroud, the standard Cathcart-Pawel correlation was used or in SOCRAT case, a mechanistic model for Zry oxidation was used. As a result, predictions of the hydrogen release rate were obtained, presented in Fig. 14. Due to differences in temperature predictions, there is a noticeable scattering in the hydrogen release rate prediction for the whole bundle even before the temperature escalation begins. The noticeable jump in the hydrogen release rate prediction by the SOCRAT code at t≈14250 s is associated with the switch from the chromium oxidation model to the zirconium oxidation model upon reaching the Cr/Zr eutectic point (1332 °C).

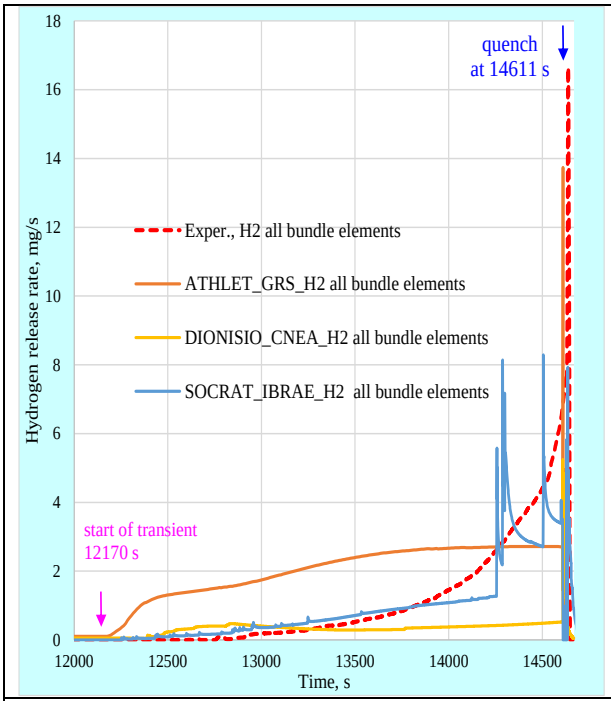

Whole bundle (coated and uncoated claddings, shroud)

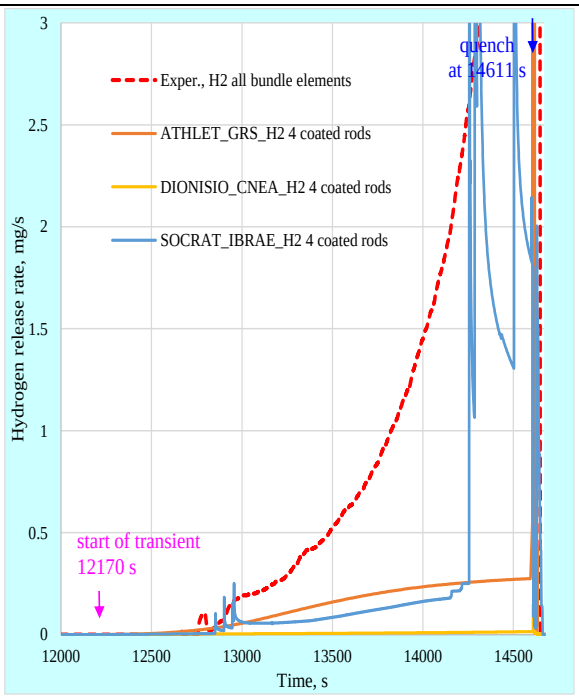

Only coated claddings

Fig. 14. Hydrogen production rates predicted for the CODEX-ATF

The corresponding integral hydrogen releases are presented in Table 4 and Fig. 15. While ATHLET-CD overestimates the hydrogen release by a factor of two (due to overpredicted temperatures for not coated claddings), the DIONISIO code underestimates the integral hydrogen release by a factor of three (temperatures were underestimated). The SOCRAT code showed the result closest to the measured values (more accurate temperature prediction and consideration of oxidation of zirconium substrates in coated tubes). A comparison of the calculated data on hydrogen release by the oxidation of zirconium and chromium shows that the predominant amount of hydrogen is associated with the oxidation of bundle parts made of Zr alloy not protected by a Cr coating.

Experiment	ATHLET/GRS	DIONISIO/CNEA	SOCRAT/IBRAE
2.91	*Zr oxidation: 4.96*	*Zr oxidation: 1.02*	*Zr oxidation: 1.57*
	Cr oxidation: 0.33	*Cr oxidation: 0.02*	*Oxidation of coated claddings: 0.91*
	total: 5.29	total: 1.04	total: 2.48

Table 4. Integral hydrogen release (in grams)

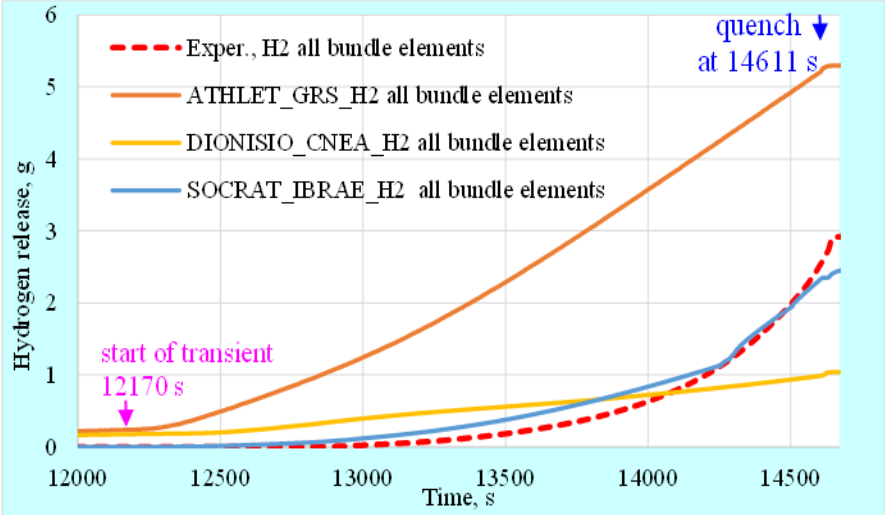

Fig. 15. Integral hydrogen release predicted for the CODEX-ATF

5. Conclusions

Benchmarks for simulating bundle experiments with ATF cladding materials, organized within the framework of the IAEA ATF-TS project, showed a good possibility of adapting codes for new materials. While the thermal-hydraulic parameters of the experiments were calculated using algorithms already built into the codes, the oxidation modules were modified to take into account the correlations of FeCrAl and Cr oxidation. The oxidation of FeCrAl included the entire operating temperature range, while the behaviour of the chromium coating was described for temperatures below the point of formation of the Cr/Zr eutectic melt. Further research is needed to take into account processes above this eutectic point.

6. Acknowledgements

This work has been conducted within the framework of IAEA's Coordinated Research Project on Testing and Simulation for Advanced Technology and Accident Tolerant Fuels (ATF-TS). The authors are grateful to Alejandro Soba, Martin Lemes and Matias Loza (CNEA), Martin Sevecek (CTU), Thorsten Hollands (GRS), Kirill Dolganov and Nikolai Ryzhov (IBRAE), Fabrizio Gabrielli (KIT), Marco Cherubini and Hector Lopez (NINE), Cesar Queral and Kevin Fernández Cosials (UPM), Kenta Inagaki (CRIEPI), Pál Kostka and Gábor Lajtha (NUBIKI) for performing pre- and post-test calculations.

7. References

[1] Kinya Nakamura, Kenta Inagaki, Naoki Tarumi, Juri Stuckert, Martin Sevecek, Behavior of bundles with Cr coated claddings under BDBA conditions at the DEGREE facility, TopFuel 2024, paper A0243.

[2] Z. Hózer, R. Farkas, N. Ver, B. Bürger, M. Sevecek, CODEX-ATF: integral bundle test with accident tolerant fuel, TopFuel 2024.

[3] INTERNATIONAL ATOMIC ENERGY AGENCY, Analysis of Options and Experimental Examination of Fuels for Water Cooled Reactors with Increased Accident Tolerance (ACTOF), IAEA-TECDOC-1921, IAEA, Vienna (2020), https://www.iaea.org/publications/14691/analysis-of-options-and-experimental-examination-of-fuels-for-water-cooled-reactors-with-increased-accident-tolerance-actof.

[4] Peter Doyle, Juri Stuckert, Mirco Grosse, Martin Steinbrück, Andrew T. Nelson, Jason Harp, Kurt Terrani, Analysis of iron-chromium-aluminum samples exposed to accident conditions followed by quench in the QUENCH-19 experiment, Journal of Nuclear Materials 580 (2023), 154433, https://doi.org/10.1016/j.jnucmat.2023.154433.

[5] Martin Steinbrueck,·Mirco Grosse,·Chongchong Tang,·Juri Stuckert, Hans Juergen Seifert, An Overview of Mechanisms of the Degradation of Promising ATF Cladding Materials During Oxidation at High Temperatures, High Temperature Corrosion of Materials, https://doi.org/10.1007/s11085-024-10229-y.

[6] Anil Gurgen, Koroush Shirvan, Estimation of coping time in pressurized water reactors for near term accident tolerant fuel claddings, Nuclear Engineering and Design 337 (2018), 38–50, https://doi.org/10.1016/j.nucengdes.2018.06.020.

[7] Chaewon Kim, Chongchong Tang, Mirco Grosse, Yunhwan Maeng, Changheui Jang, Martin Steinbrueck, Oxidation mechanism and kinetics of nuclear-grade FeCrAl alloys in the temperature range of 500–1500 °C in steam, Journal of Nuclear Materials 564 (2022), 153696, https://doi.org/10.1016/j.jnucmat.2022.153696.

[8] Kevin G. Field, Mary A. Snead, Yukinori Yamamoto, Kurt A. Terrani, Handbook on the Material Properties of FeCrAl Alloys for Nuclear Power Production Applications (FY18 Version: Revision 1), Technical Report ORNL/SPR-2018/905, 2018, https://doi.org/10.2172/1474581.

[9] J.-C. Brachet, E. Rouesne, J. Ribis, T. Guilbert, S. Urvoy, G. Nony, C. Toffolon-Masclet, M. Le Saux, N. Chaabane, H. Palancher, A. David, J. Bischoff, J. Augereau, and E. Pouillier, High temperature steam oxidation of chromium-coated zirconium-based alloys: Kinetics and process, Corrosion Science 167, 108537 (2020), https://doi.org/10.1016/j.corsci.2020.108537.

[10] J. Stuckert, M. Grosse, M. Steinbrueck, M. Walter, A. Wensauer, Results of the QUENCH-LOCA experimental program at KIT, Journal of Nuclear Materials 534 (2020), 152143, https://doi.org/10.1016/j.jnucmat.2020.152143.